ATLAS NOTE

ATLAS-CONF-2012-144

November 7, 2012

Search for supersymmetry in events with at least one photon, one lepton, and large missing transverse momentum in proton–proton collision at a center-of-mass energy of 7 TeV with the ATLAS detector

The ATLAS Collaboration

Abstract

A search for supersymmetry in events with at least one photon, one electron or muon, and large missing transverse momentum has been performed using up to 4.8 fb^{-1} of proton–proton collision data at $\sqrt{s} = 7$ TeV recorded in 2011 with the ATLAS detector. No excess of events was observed above the Standard Model prediction and model-independent exclusion limits for new physics are set. In the context of a generalized model of gauge-mediated supersymmetry breaking with a wino-like next-to-lightest supersymmetric partner, gluino masses below 619 GeV are excluded at 95 % CL for any wino mass, and wino masses below 221 GeV are excluded for any gluino mass.

1 Introduction

Supersymmetry (SUSY) [1, 2, 3, 4, 5, 6, 7, 8, 9] introduces a symmetry between fermions and bosons, resulting in a SUSY partner (sparticle) for each Standard Model (SM) particle with identical quantum numbers except a difference of half a unit of spin. As no sparticle has yet been observed, SUSY must be a broken symmetry if realised in nature. Assuming R-parity conservation [10, 11, 12, 13, 14], sparticles would be produced in pairs. These would then decay through cascades involving both other sparticles as well as SM particles until the lightest SUSY particle (LSP), which is stable, is produced.

In gauge-mediated SUSY breaking (GMSB) models [15, 16, 17, 18, 19, 20], the LSP is the gravitino ($\tilde{G}$). GMSB experimental signatures are largely determined by the nature of the next-to-lightest supersymmetric partner (NLSP). In this study the results were interpreted in the context of General Gauge Mediation (GGM) [21, 22, 23] using models where a nearly-degenerate triplet of partners of the SU(2) gauge boson, known collectively as the wino and denoted by $\tilde{\chi}_1^0$ (neutralino) and $\tilde{\chi}_1^\pm$ (chargino), serves as the NLSP. The $\tilde{\chi}_1^0$ and $\tilde{\chi}_1^\pm$ masses are so similar as to prohibit a wino state to serve as a decay product of another wino state. These states decay via $\tilde{\chi}_1^0 \to \tilde{G}(Z,\gamma)$ and $\tilde{\chi}_1^\pm \to \tilde{G}W^\pm$, leading to a substantial production rate of final states containing both a photon and a lepton accompanied by significant missing transverse momentum due to the presence of two undetected gravitinos and, in most such events, one or more neutrinos. The neutralino branching fraction to photon approaches $\sin^2\theta_W$ at high wino mass but is enhanced at lower wino mass with, for example, a value of 45 % at $m(\tilde{\chi}_1^0) = 200\,\text{GeV}$.

We performed a search for events that contain at least one photon, at least one electron or muon (including those decaying from taus), and large missing transverse momentum. The electron and muon channels were analysed separately and combined to derive model-dependent limits. The results were interpreted in a GGM framework with a wino-like NLSP. The mass of the wino and gluino ($\tilde{g}$) were treated as free parameters, with all other sparticle masses decoupled. In such a scenario, depending upon the masses of the gluino and wino states, SUSY particle production is dominated either by $\tilde{g}$-pair production (see Fig. 1) or by the production of $\tilde{\chi}_1^+\tilde{\chi}_1^-$ or $\tilde{\chi}_1^\pm\tilde{\chi}_1^0$ pairs (see Fig. 2). In the former case, the gluinos decay via cascades into the wino-like charged and neutral NLSPs, accompanied by other SM particles such as gluons, quarks, leptons and gauge bosons. A prior study by the CMS collaboration [24] within the context of this model set a 95 % CL lower limit on $m(\tilde{g})$ of 440 GeV for any value of the wino mass.

Potential SM backgrounds are expected to be dominated by the production of a W boson or $t\bar{t}$ pair in association with a photon ($W\gamma$, $t\bar{t}\gamma$), and $t\bar{t}$ production for which both top quarks decay semileptonically and one lepton, an electron, is misidentified as a photon (referred to as fully-leptonic $t\bar{t}$). Background

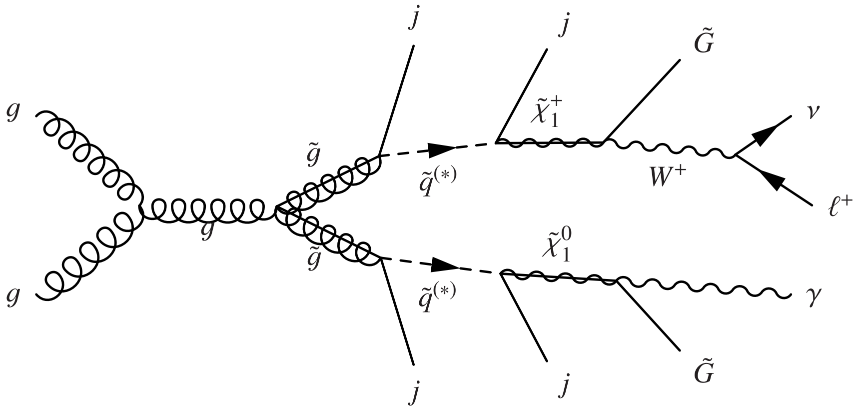

Figure 1: Example of gluino production and subsequent decay to a final state with a photon, lepton, and missing transverse momentum.

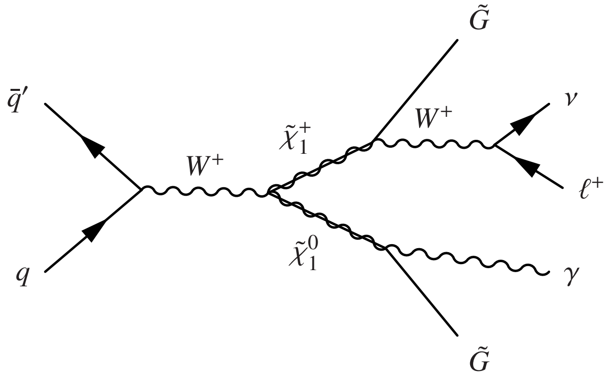

Figure 2: Example of direct s-channel wino-like chargino-neutralino production and subsequent decay to a final state with a photon, lepton, and missing transverse momentum.

contributions from these sources were estimated via Monte Carlo simulation (MC). Background events can also arise from SM processes involving jets, such as W + jets, semi-leptonic $t\bar{t}$, γ + jets, and $Z(\rightarrow \mu\mu)$ + jets, for which one of the jets is misidentified as a photon or a lepton candidate. Data-driven methods were employed to model such backgrounds. Other, less important backgrounds, like other $Z + X$, single-top, and other diboson (WW,WZ, and ZZ) events were modeled by MC.

2 ATLAS Detector

The ATLAS detector [25] is a multi-purpose apparatus with a forward-backward symmetric cylindrical geometry and nearly 4π solid angle coverage. Closest to the beamline are tracking devices comprising layers of silicon-based pixel and strip detectors covering $|\eta| < 2.5$[1] and straw-tube detectors covering $|\eta| < 2.0$, located inside a thin superconducting solenoid that provides a 2 T magnetic field. The straw-tube detectors also provide discrimination between electrons and charged hadrons based on transition radiation. Outside the solenoid, fine-granularity lead/liquid-argon electromagnetic (EM) calorimeters measure the energy and position of electrons and photons in the region $|\eta| < 3.2$. A presampler, covering $|\eta| < 1.8$, is used to correct for energy lost by particles before entering the EM calorimeter. An iron/scintillating-tile hadronic calorimeter covers the region $|\eta| < 1.7$, while copper and liquid-argon technology is used for hadronic calorimeters in the end-cap region $1.5 < |\eta| < 3.2$. In the forward region $3.2 < |\eta| < 4.9$ liquid-argon calorimeters with copper and tungsten absorbers measure the electromagnetic and hadronic energy. A muon spectrometer (MS) consisting of three superconducting toroidal magnet systems each comprising eight toroidal coils, tracking chambers, and detectors for triggering surrounds the calorimeter system.

The ATLAS detector uses three levels of triggering [26]. Level 1 is implemented in custom hardware and has to perform decisions quickly. Layer 2 is implemented in software using simple algorithms. Finally, the high-level trigger (HLT) uses simplified versions of the standard reconstruction algorithms to make the final selections.

---

[1] ATLAS uses a right-handed coordinate system with its origin at the nominal interaction point (IP) in the centre of the detector and the z-axis along the beam pipe. The x-axis points from the IP to the centre of the LHC ring, and the y-axis points upward. Cylindrical coordinates (r, ϕ) are used in the transverse plane, ϕ being the azimuthal angle around the beam pipe. The pseudorapidity is defined in terms of the polar angle θ as $\eta = -\ln\tan(\theta/2)$.

3 Monte Carlo Simulated Samples

Simulated samples of signal events, used for optimizing selection cuts and for estimating selection efficiency, were generated in the context of a GGM model with a wino-like neutralino NLSP. The model was simplified in the sense that only the key features of the GGM scenario were modeled without considering, for example, the details of the mass spectrum or the potential origin of the model. These key features are determined by the mass of the wino, set by the model parameter M_2, and, for strong production, by the mass of the gluino, set by M_3. These two parameters were allowed to take a range of values that covered the expected sensitive range of this search. (See Ref. [21] for the model parameter definitions in more detail.) More specifically, MC samples were generated with M_3 set to 600 GeV, 700 GeV, 800 GeV, 900 GeV, 1000 GeV and 1500 GeV, and with M_2 varied from 100 GeV to $M_3 - 20$ GeV for $M_3 \leq 800$ GeV and 100 GeV to 400 GeV for $M_3 > 800$ GeV. The model parameters that control the other gaugino masses, M_1 and μ, and the squark and slepton masses were set to 2.5 TeV. The lifetime of the NLSP was set to ensure prompt decays ($c\tau_{NLSP} < 0.1$ mm). The full mass spectrum and the gluino branching fractions and decay width were calculated from this set of parameters using SUSPECT 2.41 [27], SDECAY 1.3B1 [28], and HDECAY 3.41 [29]. Simulated events were generated with HERWIG++ [30]. Cross sections for signal processes involving the production of gluino pairs were calculated to next-to-leading order (NLO) in the strong coupling constant, adding the resummation of soft gluon emission at next-to-leading-logarithmic accuracy (NLO+NLL) [31, 32, 33, 34, 35]. Cross sections for signal processes involving the production of wino pairs were calculated to NLO using PROSPINO2 [31]. In both cases, the nominal cross section and the uncertainty were taken from an envelope of cross section predictions using different PDF sets and factorisation and renormalisation scales, as described in Ref. [36]. The calculated cross section for a point with $m(\tilde{g}) = 1500$ GeV and $m(\tilde{\chi}_1^0) = 200$ GeV, which is dominated by electroweak-strength production, is 0.94 ± 0.04 pb, and for a point with $m(\tilde{g}) = 600$ GeV and $m(\tilde{\chi}_1^0) = 500$ GeV, dominated by strong production, it is 0.68 ± 0.13 pb.

Expected SM backgrounds were simulated as follows. The ALPGEN [37] MC generator with the CTEQ6L1 PDF [38] was used to simulate $W\gamma$ events, with a requirement that the momentum of the photon in the plane transverse to the beam direction (p_{T}) satisfy $p_{\mathrm{T}} > 40$ GeV. ALPGEN matrix elements were generated with up to five partons, and MLM matching [37] was used to interface the matrix elements to HERWIG for parton showering and fragmentation. The $W\gamma$ cross section was normalized to the value measured in Ref. [39]. GGM signal contamination would be negligible in the selection used to measure the cross section. The WHIZARD [40] MC generator with the CTEQ6L1 PDF was used to simulate $t\bar{t}\gamma$ events, requiring that at least one photon has $p_{\mathrm{T}} > 8$ GeV, and excluding events for which both top quarks decay hadronically. HERWIG was used for parton showering and fragmentation, with additional photon radiation added via PHOTOS [41]. To account for higher-order processes, the cross section measured from WHIZARD was multiplied by a k-factor of 2.55 ± 0.50 [42]. The MC@NLO [43, 44] generator, including full NLO QCD corrections, was used to simulate $t\bar{t}$ production. The CTEQ6.6m PDF [45] was used. The $t\bar{t}$ cross section was estimated at next-to-next-to-leading-order (NNLO) using Hathor 1.2 [46], making use of the MSTW2008 90 % NNLOPDF sets [47]. To avoid double-counting with the $t\bar{t}\gamma$ sample, events with a photon with $p_{\mathrm{T}} > 8$ GeV and invariant masses between massless matrix-element partons greater than 5 GeV were removed from the $t\bar{t}$ samples. $Z\gamma$ events were generated with SHERPA [48], requiring that at least one photon has $p_{\mathrm{T}} > 40$ GeV. The electron and muon events were generated with the CTEQ6.6M PDF while the tau events used CT10 [49]. The normalization is as calculated by SHERPA. $W+$jets and $Z+$jets events were generated with ALPGEN, with matrix elements including up to five partons, and interfaced to HERWIG for the simulation of showering and fragmentation, and used the CTEQ6L1 PDF. The $Z+$jets sample was normalized to the inclusive Z boson cross section calculated at NNLO in QCD via the FEWZ [50] program. $W+$ jets events with a photon with $p_{\mathrm{T}} > 40$ GeV were removed to avoid overlap with the $W\gamma$ sample. Similarly, $Z+$jets events with $p_{\mathrm{T}} > 40$ GeV and the same

$\Delta R(e, \gamma)$ selection as used to generate the $Z\gamma$ MC sample (which differed for e/μ and τ) were removed to avoid double-counting. Two separate single-top production processes were simulated. Wt events were generated using MC@NLO, including full NLO QCD corrections, and interfaced to HERWIG for the simulation of showering and fragmentation. The CTEQ6.6m PDF was used. Single-top events produced via t-channel processes were generated with the AcerMC [51] MC generator, with parton showering and fragmentation performed by PYTHIA, and with the final-state W boson decaying leptonically. The LO**, LHAPDF 20651 modified LO PDFs [52] were used. The reference cross sections were taken from Ref. [53] and Ref. [54], respectively. The background from single-top events produced via the s-channel was found to be negligible. Diboson (WW, WZ, and ZZ) events were generated with SHERPA using the CT10 PDF, with cross sections provided by MCFM [55]. A $\gamma\gamma$ sample was also generated by SHERPA, with the LO cross section enhanced by a k-factor of 1.2. Samples making use of PYTHIA [56] and HERWIG [57, 58] use a set of parameters tuned by ATLAS for its 2011 Monte Carlo generation [59]. For signal and background samples making use of HERWIG, JIMMY [60] was used to simulate activity due to the underlying event.

All signal and background samples were passed through a GEANT4-based simulation of the ATLAS detector [61, 62] and were reconstructed with the same algorithms used for the data. The variation of the number of pp interactions per bunch crossing (pile-up) as a function of the instantaneous luminosity was taken into account by overlaying simulated minimum bias events according to the observed distribution of the number of pile-up interactions in data, with an average of ~10 interactions.

4 Object Definitions

The reconstruction of converted and unconverted photons is described in Ref. [63]. Converted photons have tracks from a conversion vertex matching a cluster of cells in the calorimeter, while unconverted ones do not. For comparison, electrons have a track matched to the cluster. An object that originates from one cluster of cells in the calorimeter can be considered as both a photon and an electron.

Photon candidates were required to be within $|\eta| < 2.37$, and to be outside the transition region $1.37 < |\eta| < 1.52$ between the barrel and end-cap calorimeters. The standard signal photons were required to pass the 'TightAR' criteria, which makes use of the characteristics of the longitudinal and transverse shower development in the EM calorimeter to separate photons from jets. Fine granularity in η in the first layer of the calorimeter was used to reject π^0 mesons. Furthermore, as part of the TightAR criteria, in the case that a calorimeter cluster was identified as both a photon and an electron, a classification algorithm based on the electron track and the conversion track and vertex qualities, if any, was applied, and the object was potentially classified as a photon only if the photon interpretation was preferred. Additionally, even if the algorithm favored the photon interpretation, if the object interpreted as an electron fulfilled all the signal electron criteria, then the electron interpretation was chosen.

An isolation requirement was imposed on the signal photons. Photon candidates were removed if more than 5 GeV of transverse energy was observed in a cone of $\Delta R \equiv \sqrt{(\Delta\eta)^2 + (\Delta\phi)^2} < 0.2$ surrounding the photon's deposition in the calorimeter, after correcting for contributions from pile-up and the E_{T} leakage from the photon itself,

The reconstruction of electrons is described in Ref. [64]. Electron candidates were required to be within $|\eta| < 2.47$, again excluding the transition region $1.37 < |\eta| < 1.52$. Signal electrons were required to pass the 'medium++' selection criteria, which is based on the characteristics of the EM shower development, the quality of the associated reconstructed track, and the closeness of the match between the track and the calorimeter deposition. Electron candidates were removed if more than 10% of the electron's p_{T} was contained in tracks in a cone of $\Delta R < 0.2$ after removing the track ascribed to the electron itself.

The reconstruction of muons is described in [65]. A reconstructed track was identified as having arisen from the passage of a muon if it met statistical requirements for its combination with a track from the MS, or for its consistency with the location of several MS hits. Muon candidates were required to be within $|\eta| < 2.4$, and the signal muons were required to have the sum of track p_{T} contained in a cone of size $\Delta R < 0.2$ be less then 1.8 GeV, after removing the track of the muon itself.

Jets were reconstructed using the anti-k_{T} jet algorithm [66] with four-momentum recombination and distance parameter $R = 0.4$. They were required to have $p_{\mathrm{T}} > 20$ GeV [67]. The analysis made no explicit jet requirement.

The measurement of the two-dimensional transverse momentum vector $\mathbf{p}_{\mathrm{T}}^{\mathrm{miss}}$ (and its magnitude $E_{\mathrm{T}}^{\mathrm{miss}}$) was based on energy deposits in calorimeter cells inside three-dimensional clusters with $|\eta| < 4.5$. The cluster energy was calibrated to correct for the different response to electromagnetically- and hadronically-induced showers, energy loss in dead material, and out-of-cluster energy. The contribution from identified muons was accounted for by subtracting the small energy deposit of the muon in the calorimeter and adding the muon object p_{T} [68].

5 Event Selection and Background Modeling

This analysis used 4.8 fb^{-1} of data in the electron channel and 4.7 fb^{-1} in the muon channel. Electron-channel candidate events were selected by a trigger requiring at least two loose electron or photon candidates, each with a transverse energy $E_{\mathrm{T}} > 20$ GeV. In earlier running periods, muon-channel candidate events were selected by a trigger requiring at least one muon with $p_{\mathrm{T}} > 18$ GeV. In later periods, in order to maintain a tractable trigger rate with the increased instantaneous luminosity, a jet requirement in the first level of the trigger with $E_{\mathrm{T}} > 10$ GeV was added to the muon requirement. (The photon fires the jet part of the trigger with nearly full efficiency.) To ensure that the candidate events resulted from a beam collision, they were required to have at least one primary vertex candidate with five or more associated tracks, and several event cleaning criteria were applied to veto events that were likely from beam halo or cosmic ray muons or from detector noise [67].

A simple truth-level optimization was performed to find the photon p_{T}, $E_{\mathrm{T}}^{\mathrm{miss}}$, and m_{T} requirements that maximized the expected signal significance, $\sqrt{2[(s + b)\ln(1 + s/b) - s]}$, where s and b are the expected signal and background abundances. The signal point used for the optimization was with $m(\tilde{g}) = 600$ GeV and $m(\tilde{\chi}_1^0) = 200$ GeV, where the low mass of the wino was chosen to improve the sensitivity in the expected reach for electroweak production.

Electron-channel candidate events were required to have at least one isolated photon with $p_{\mathrm{T}} > 100$ GeV, at least one isolated electron with $p_{\mathrm{T}} > 25$ GeV, no identified muons with $p_{\mathrm{T}} > 25$ GeV, and $|m_{e\gamma} - m_Z| > 15$ GeV, where $m_Z = 91.2$ GeV is the Z-boson mass. Muon-channel candidate events were required to have at least one isolated photon with $p_{\mathrm{T}} > 85$ GeV, at least one isolated muon with $p_{\mathrm{T}} > 25$ GeV, and no identified electrons with $p_{\mathrm{T}} > 25$ GeV. The somewhat-relaxed value of the muon-channel photon p_{T} cut reflects the lower background in the muon channel. Both electron- and muon-channel candidate events were further required to have a minimum angular separation $\Delta R(\ell, \gamma) > 0.7$ between the leading lepton and photon candidates.

The $\gamma + \ell + E_{\mathrm{T}}^{\mathrm{miss}}$ events were further separated into mutually-exclusive signal and control samples through requirements on $E_{\mathrm{T}}^{\mathrm{miss}}$ and the transverse mass (m_{T}), defined as

$$m_{\mathrm{T}} = \sqrt{2 p_{\mathrm{T}}^{\ell} E_{\mathrm{T}}^{\mathrm{miss}} \left(1 - \cos \Delta\phi_{\ell, \mathbf{p}_{\mathrm{T}}^{\mathrm{miss}}}\right)} \tag{1}$$

where ℓ refers to either the electron or muon. W boson events exhibit an edge at $m_{\mathrm{T}} = m_W$, so requiring large m_{T} suppresses the dominant $W + X$ background. The selection requirements, $E_{\mathrm{T}}^{\mathrm{miss}} > 100$ GeV and $m_{\mathrm{T}} > 100$ GeV, define the signal region (SR). The presence of energetic gravitinos and neutrinos tends to produce substantial $E_{\mathrm{T}}^{\mathrm{miss}}$ in GGM events, and GGM events are not subject to the m_{T} edge but tend to instead have higher values of m_{T}. A W-boson-rich control region (WCR) was defined via intermediate requirements on both $E_{\mathrm{T}}^{\mathrm{miss}}$ and m_{T}. A high-$E_{\mathrm{T}}^{\mathrm{miss}}$ control region (HMET) required a value of $E_{\mathrm{T}}^{\mathrm{miss}}$ of at least 80 GeV – nearly as large as that of the signal region – but that the value of m_{T} be intermediate (so as to be orthogonal to the SR). Similarly, a high-m_{T} control region (HMT) was defined by requiring large m_{T} but intermediate $E_{\mathrm{T}}^{\mathrm{miss}}$. The requirements for the signal and control regions are summarized in Table 1.

Signal or Control Region	$E_{\mathrm{T}}^{\mathrm{miss}}$ [GeV]		m_{T} [GeV]	
	low	high	low	high
SR	100	—	100	—
WCR	35	80	35	90
HMET	80	—	35	90
HMT	35	80	90	—

Table 1: Requirements applied to $E_{\mathrm{T}}^{\mathrm{miss}}$ and m_{T} to define the signal region (SR) and various control regions (WCR, HMET, HMT) discussed in the text.

Including the lepton-plus-photon branching fraction, the SR acceptance for a point with $m(\tilde{g})$ = 1500 GeV and $m(\tilde{\chi}_1^0)$ = 200 GeV is $(2.6 \pm 0.1) \times 10^{-3}$ in the electron channel and $(2.9 \pm 0.1) \times 10^{-3}$ in the muon channel. The errors given are due to MC sample statistics; further uncertainties are discussed in Section 6. The greater acceptance in the muon channel is as a result of the lower photon p_{T} requirement in that channel. The acceptance for a point with $m(\tilde{g})$ = 600 GeV and $m(\tilde{\chi}_1^0)$ = 500 GeV is $(6.5 \pm 0.3) \times 10^{-3}$ in the electron channel and $(4.0 \pm 0.2) \times 10^{-3}$ in the muon channel. In this case, because of the larger wino mass, the photon p_{T} spectrum is harder, so there is little penalty in the electron channel from requiring $p_{\mathrm{T}} > 100$ GeV, while the electron channel benefits from a higher identification and trigger acceptance.

Dominant backgrounds arise from $W\gamma$, $t\bar{t}\gamma$, and fully-leptonic $t\bar{t}$ production; in the latter case the signature arises through the misidentification of an electron as a photon. These backgrounds were estimated via MC. The rate of electron-to-photon misidentification was found to be well-modeled by a comparison of the rate of reconstructing $Z \to e\gamma$ in both data and MC. Smaller backgrounds arising from single-top, Z boson, and diboson production were also modeled via MC. The systematic uncertainties associated with the precision of the modeling of these backgrounds are discussed in Section 6.

The rate of jets being misidentified as photons is not modeled sufficiently accurately in the MC. Therefore, the backgrounds from jets misidentified as photons, which arise from W + jets and semi-leptonic $t\bar{t}$ events, were estimated with the data driven method referred to as the "ABCD method." In that method, regions A, B, C, and D were defined to contain those events for which the leading photon was tight (tightAR) and isolated, tight and non-isolated, anti-tight and isolated, and anti-tight and non-isolated, respectively. Anti-tight photons are defined as photons that pass the tight photon criteria in the second layer of the EM calorimeter but fail some criteria in the first layer. To the extent that all of the events in regions B, C, and D arose from events for which the leading photon candidate is a mis-reconstructed jet, the number of events in sample A arising from jets mis-reconstructed as photons would be given by

$$N_A^{j\to\gamma} = \frac{N_B N_C}{N_D} \tag{2}$$

where N_X represents the number of events in region X. This expression assumes no correlation between the jet misidentification rate of isolated and non-isolated photons, so that $N_A/N_C = N_B/N_D$. In the analysis corrections for control-region contributions from other processes and from correlations between isolated and non-isolated photons were accounted for using MC, implemented according to Ref. [39].

The number of data events, however, was too small to apply the ABCD method directly in the SR.

Instead, the method was applied to the various control samples both individually and inclusively. In the electron channel, the photon p_{T} cut was further reduced to 50 GeV to increase the event yield. The W + jets and semi-leptonic $t\bar{t}$ MC was scaled to match the predicted yield in the control regions, and the same scale was applied to the MC in the SR to arrive at the estimate there.

The background from γ + jets events was estimated via the so-called matrix method, in which one solves the system of equations

$$\begin{aligned} N_{\mathrm{loose}} &= N_{\mathrm{loose}}^{\mathrm{true}} + N_{\mathrm{loose}}^{\mathrm{misid}} && (3) \\ N_{\mathrm{tight}} &= \varepsilon^{\mathrm{true}} N_{\mathrm{loose}}^{\mathrm{true}} + \varepsilon^{\mathrm{misid}} N_{\mathrm{loose}}^{\mathrm{misid}} && (4) \end{aligned}$$

where N_{tight} (N_{loose}) is the number of candidate events accumulated under the requirement that the lepton candidate satisfy tight (loose) identification criteria and $\varepsilon^{\mathrm{true}}$ ($\varepsilon^{\mathrm{misid}}$) represents the fraction of true (misidentified) leptons that pass the tight selection, given that they also pass the loose selection. An estimate of $\varepsilon^{\mathrm{true}}$ was obtained from $Z \to ee$ or $Z \to \mu\mu$ events. The value of $\varepsilon^{\mathrm{misid}}$ was estimated using a sample of events requiring a loose lepton and with $E_{\mathrm{T}}^{\mathrm{miss}} \lesssim 20$ GeV and $m_{\mathrm{T}} \lesssim 20$ GeV, but otherwise satisfying the signal region selection criteria. The actual $E_{\mathrm{T}}^{\mathrm{miss}}$ and m_{T} cut values were varied to check for stability, and real lepton leakage was subtracted using MC.

The efficiency of the diphoton trigger required of electron-channel events was estimated using a bootstrap method [26]. The muon trigger efficiency and uncertainty was used as parametrized for Ref. [69].

Tables 2 and 3 show the background predictions in the various control regions for the electron and muon channels, respectively. Uncertainties are due to MC or data statistics only; systematic uncertainties will be discussed in the next section. Also shown are the observed numbers of events for each region. They are found to agree with the expectation.

Yields	WCR	HMT	HMET
$W\gamma$	106.3 ± 3.1	43.7 ± 2.0	60.6 ± 2.3
W + jets	9.5 ± 1.0	3.0 ± 0.5	8.6 ± 0.9
$t\bar{t}\gamma$	7.8 ± 0.4	3.5 ± 0.3	7.1 ± 0.4
fully-leptonic $t\bar{t}$	3.6 ± 0.4	3.7 ± 0.4	2.3 ± 0.3
semi-leptonic $t\bar{t}$	0.5 ± 0.1	0.2 ± 0.0	0.3 ± 0.1
single top	0.7 ± 0.3	1.1 ± 0.3	0.9 ± 0.3
WW, WZ, ZZ	1.5 ± 0.2	1.8 ± 0.2	1.2 ± 0.2
$Z\gamma$	4.2 ± 0.3	4.6 ± 0.2	0.7 ± 0.1
Z + jets	4.3 ± 1.1	5.0 ± 1.2	0.2 ± 0.2
diphoton	18.5 ± 2.9	12.2 ± 2.4	0.5 ± 0.5
γ + jets	33.6 ± 3.2	20.1 ± 2.4	1.5 ± 0.9
total predicted	190.6 ± 5.6	98.8 ± 4.2	83.9 ± 2.8
data	195	104	71

Table 2: Numbers of expected background and observed data events for the electron channel in the different control regions. Only statistical uncertainties are given.

Figures 3 and 4 show, separately for the electron and muon channels, the $E_{\mathrm{T}}^{\mathrm{miss}}$ and m_{T} distributions for the various control regions. The expected backgrounds are represented as stacked histograms. Also shown are the signal distributions for a signal with ($m(\tilde{g})$ = 600 GeV; $m(\tilde{\chi}_1^0)$ = 500 GeV) and ($m(\tilde{g})$ = 1500 GeV; $m(\tilde{\chi}_1^0)$ = 200 GeV) after satisfying all selection criteria. In all cases, the background is found to agree with the data in both shape and normalisation.

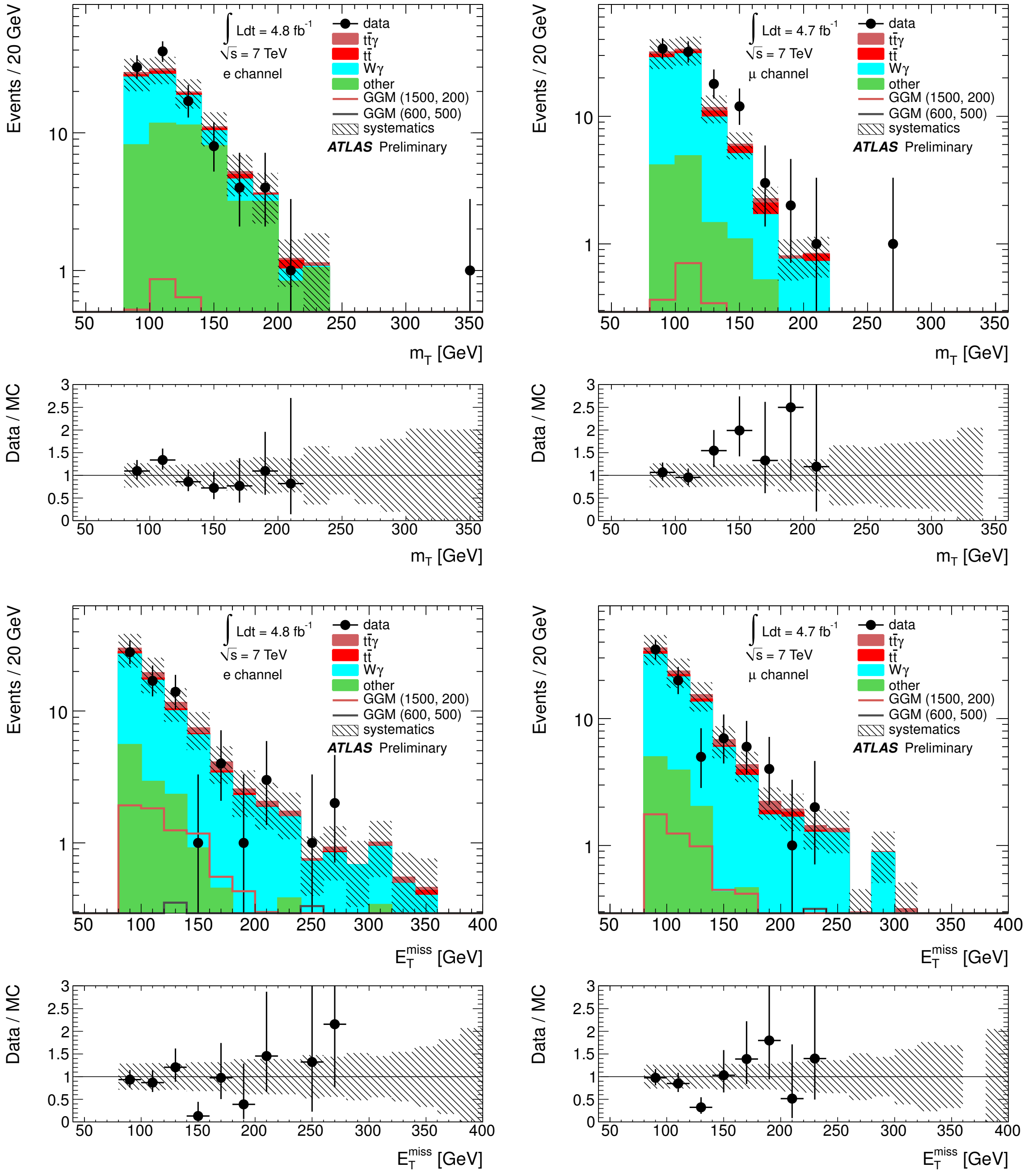

Figure 3: The m_{T} distributions of the HMT samples (top) and the $E_{\mathrm{T}}^{\mathrm{miss}}$ distributions of the HMET samples (bottom) for the electron (left) and muon (right) channels. The composition of the background estimates and the signal are shown, with the hashing approximating the systematic uncertainties of the background modeling. The error bars represent the Poisson statistical uncertainties of the data. Also shown are the signal distributions for ($m(\tilde{g})$ = 600 GeV; $m(\tilde{\chi}_1^0)$ = 500 GeV) and ($m(\tilde{g})$ = 1500 GeV; $m(\tilde{\chi}_1^0)$ = 200 GeV).

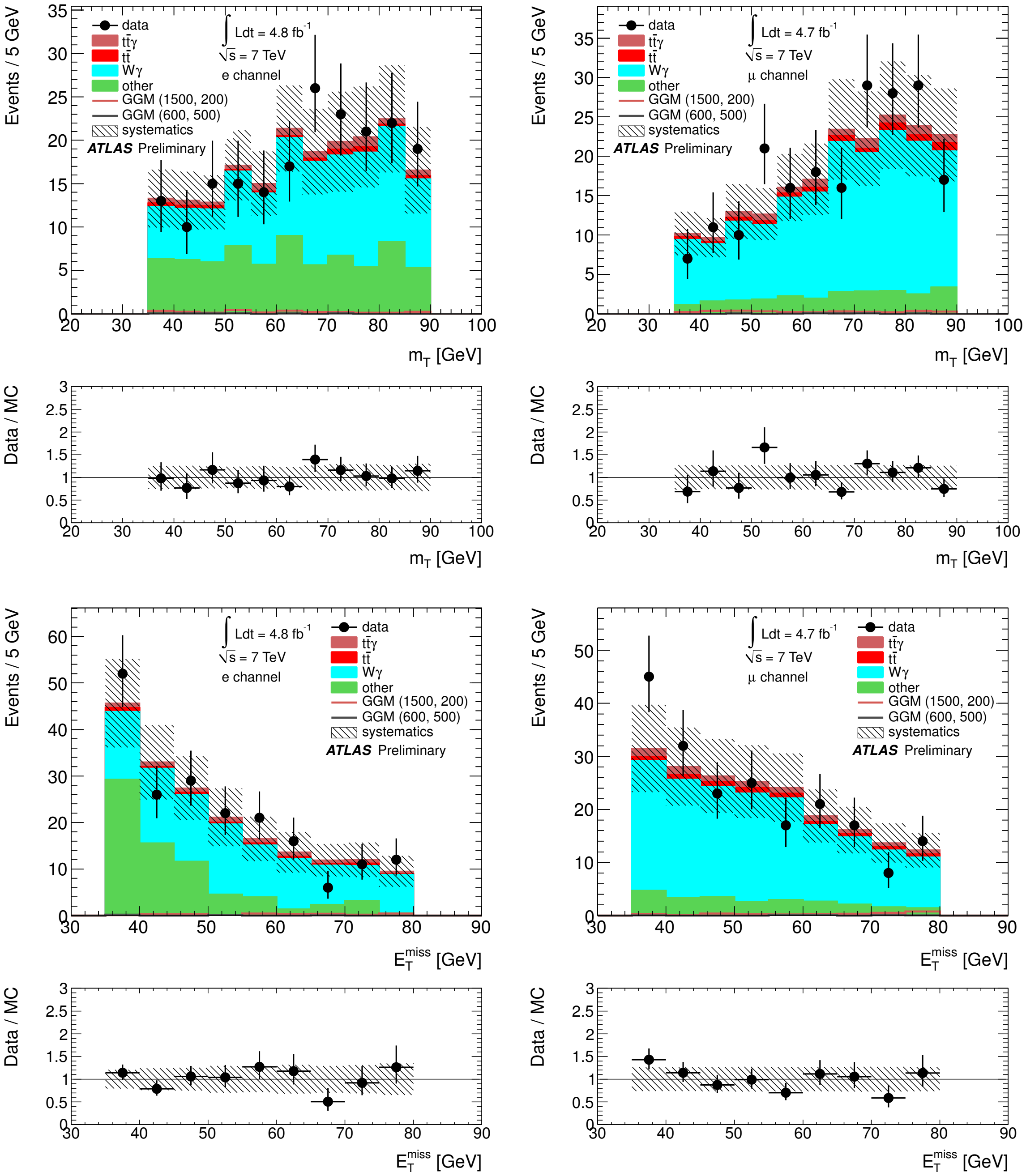

Figure 4: The m_{T} (top) and $E_{\mathrm{T}}^{\mathrm{miss}}$ (bottom) distributions of the WCR samples for the electron (left) and muon (right) channel. The composition of the background estimates and the signal are shown, with the hashing approximating the systematic uncertainties of the background modeling. The error bars represent the Poisson statistical uncertainties of the data. Also shown are the signal distributions for ($m(\tilde{g}) = 600\,\mathrm{GeV}$; $m(\tilde{\chi}_1^0) = 500\,\mathrm{GeV}$) and ($m(\tilde{g}) = 1500\,\mathrm{GeV}$; $m(\tilde{\chi}_1^0) = 200\,\mathrm{GeV}$).

Yields	WCR	HMT	HMET
$W\gamma$	154.6 ± 3.3	65.7 ± 2.2	71.6 ± 2.3
W + jets	13.4 ± 0.8	4.9 ± 0.5	7.7 ± 0.7
$t\bar{t}\gamma$	9.6 ± 0.4	4.0 ± 0.3	7.2 ± 0.3
fully-leptonic $t\bar{t}$	6.4 ± 0.5	5.1 ± 0.4	3.6 ± 0.4
semi-leptonic $t\bar{t}$	0.5 ± 0.1	0.2 ± 0.0	0.4 ± 0.0
single top	2.0 ± 0.4	1.0 ± 0.3	1.3 ± 0.3
WW, WZ, ZZ	2.0 ± 0.2	1.9 ± 0.2	1.1 ± 0.2
$Z\gamma$	6.2 ± 0.3	3.5 ± 0.2	1.5 ± 0.1
Z + jets	0.6 ± 0.2	0.4 ± 0.2	0.2 ± 0.1
γ + jets	0.8 ± 1.1	1.1 ± 1.0	0.3 ± 0.7
total predicted	196.1 ± 3.7	87.8 ± 2.6	95.0 ± 2.6
data	202	103	80

Table 3: Numbers of expected background and observed data events for the muon channel in the different control regions. Only statistical uncertainties are given.

6 Systematic Uncertainties

Systematic uncertainties arose in the estimation of the delivered luminosity (3.9 % [70, 71]), in the modeling of backgrounds, the estimation of the signal acceptance as a function of gluino and wino mass, and in the calculation of the signal cross sections.

For the modeling of backgrounds, an important systematic uncertainty stemmed from the background fiducial cross section estimates, with that of $W\gamma$ being the dominant one. The $W\gamma$ cross section was normalized to the measured value for $p_{\mathrm{T}} > 60\,\mathrm{GeV}$ and any number of jets [39], and the 9.5 % uncertainty in the measured cross section was applied as an uncertainty to the background model. Another 15 % uncertainty was added to account for differences in the MC normalization factor calculated for different values of jet multiplicity and photon p_{T}. A further uncertainty of 21% was added to cover differences in the $W\gamma$ yield in the SR predicted by the `SHERPA` and `ALPGEN` MC generators. These sources of systematic effects led to an uncertainty of 1.7 (2.4) events in the electron-channel (muon-channel) background prediction.

Also significant was the uncertainty on the fiducial $t\bar{t}\gamma$ cross section. The rate of $t\bar{t}\gamma$ production was scaled by a factor of 2.55 ± 0.50 to account for NLO QCD corrections [42, 72], where the uncertainty is from a comparison of the k-factors calculated at renormalization scales of m_t and $m_{t\bar{t}}$. The resulting 20 % uncertainty was doubled to 40 % to take into account possible additional uncertainties arising from the stringent SR selection. This uncertainty corresponds to an uncertainty of 0.9 events in both the electron- and muon-channel background predictions.

The fully-leptonic $t\bar{t}$ fiducial cross section uncertainty was found to be 0.2 (0.3) events in the electron-channel (muon-channel) background prediction, and the W+jets uncertainty was 0.3 events. The W+jets uncertainty includes uncertainties related to the ABCD method, though the theory uncertainties dominate. Smaller uncertainties arose from the uncertainty in the fiducial cross sections of other contributing background channels, mainly Z, diboson, single top, and semi-leptonic $t\bar{t}$.

Another important uncertainty in the MC background modeling was due to the $E_{\mathrm{T}}^{\mathrm{miss}}$ and m_{T} selection of the SR. Reconstructed values for $E_{\mathrm{T}}^{\mathrm{miss}}$ and m_{T} are affected by uncertainties in the calorimeter energy scale and in the muon momentum scale. The $E_{\mathrm{T}}^{\mathrm{miss}}$ and m_{T} uncertainties were treated together and assumed to be fully correlated. The clusters in the calorimeter had their energy scale shifted up and down by their uncertainties in order to evaluate the systematic effects in the SR. As an example, this produced an uncertainty of +28.0 % −21.2 % (+13.2 % −9.8 %) in the electron (muon) channel for the $W\gamma$ sample. Furthermore, the p_{T} of the muon used in the $E_{\mathrm{T}}^{\mathrm{miss}}$ calculation was smeared and the $E_{\mathrm{T}}^{\mathrm{miss}}$ and m_{T} were recalculated. The uncertainty was negligible in the electron channel, but for the $W\gamma$ sample, an uncertainty of 2.7 % was found in the muon channel. The $E_{\mathrm{T}}^{\mathrm{miss}}$ and m_{T} uncertainties for the $t\bar{t}\gamma$ and fully-leptonic $t\bar{t}$ samples were found to be of similar size. The resulting uncertainty in the total background prediction arising from the $E_{\mathrm{T}}^{\mathrm{miss}}$ and m_{T} requirements was found to be 2.4 (2.0) events in the electron-channel (muon-channel) in the SR.

An uncertainty of 4.0 % was assigned to the photon reconstruction efficiency by comparing the efficiency predicted by a data-driven method [63] and the standard method, which shifts the photon shower variables of the MC samples to have the same mean as the corresponding variables of photons in data. An uncertainty of 1.8 % arose from possible mismodeling of the rate of reconstructing a converted photon as unconverted and vice versa, and an uncertainty of 1.0 % was added due to the uncertainty on the efficiency of the photon isolation requirement [73]. Varying the photon energy scale by its uncertainty [64] yielded an uncertainty of 1.3 % to 4.0 % on the different backgrounds, and varying the energy resolution yielded an uncertainty of 1.0 %. Together, the photon efficiencies resulted in uncertainty of 0.6 (0.8) events in the electron-channel (muon-channel) background modeling.

An uncertainty of 0.2 events was assigned to the electron-channel background modeling to account for possible mismodeling of the electron-reconstruction efficiency [64], and 0.3 events due to the trigger. Similarly, an uncertainty of 0.3 events was assigned to the muon channel background modeling to account for for possible mismodeling of the muon-reconstruction [65, 74] and trigger efficiencies.

A relative uncertainty of 4.4 % was ascribed to the imprecise knowledge of the mean number of pile-up interactions per event, leading to a further uncertainty of 0.6 (0.7) events in the electron-channel (muon-channel) background prediction. In the electron channel, a γ + jets uncertainty of 0.3 events was also added, dominated by the limited statistics used in the SR to which the matrix method was applied. Including all the systematics effects mentioned above with the luminosity uncertainty and MC statistical uncertainties of 1.2 (0.9) events results in a total systematic uncertainty of 3.4 (3.6) events in the background modeling of the electron-channel (muon-channel). Table 4 summarizes the systematic uncertainties per background source.

Several of the systematic uncertainties in the background modeling also apply to the signal efficiency and acceptance, with the dominant sources summarized in Table 5 for two characteristic points in the signal parameter space. The $m(\tilde{g}) = 1500\,\mathrm{GeV}$, $m(\tilde{\chi}_1^0) = 200\,\mathrm{GeV}$ point is dominated by electroweak production while the $m(\tilde{g}) = 600\,\mathrm{GeV}$, $m(\tilde{\chi}_1^0) = 500\,\mathrm{GeV}$ point is dominated by strong production. The uncertainty on the signal acceptance due to the correlated $E_{\mathrm{T}}^{\mathrm{miss}}$ and m_{T} uncertainties varies between $(20-40)$ % for small wino masses to $(1-2)$ % for larger wino masses. For low wino masses the $E_{\mathrm{T}}^{\mathrm{miss}}$ and m_{T} requirements fall in the center of the distributions, hence the large uncertainties, while the cuts are in the tails of distributions for large wino masses. The photon systematics are the same as in the background modeling, except that the uncertainty in the photon energy scale produced variation from < 0.1 % for large wino masses to as much as 3.0 % for lower wino masses. The effect of the imprecise knowledge of the mean number of pile-up interactions per event was studied and found to be negligible.

The theoretical uncertainty on the estimation of the production cross section of the signal was estimated as outlined in Ref. [36]. The magnitude of this uncertainty varies from as little as 4 % for low wino mass and high gluino masses, for which the cross section is dominated by electroweak production, to as much as 26 % for points for which both the gluino and wino masses are large, for which strong production dominates.

Yields	electron channel	muon channel
$W\gamma$	$6.1^{+2.5}_{-2.3}$	$8.6^{+2.9}_{-2.8}$
$W+\text{jets}$	0.5 ± 0.4	$0.3^{+0.4}_{-0.3}$
$t\bar{t}\gamma$	2.2 ± 1.0	2.3 ± 1.0
fully-leptonic $t\bar{t}$	1.5 ± 0.4	$2.3^{+0.6}_{-0.8}$
semi-leptonic $t\bar{t}$	$0.02^{+0.06}_{-0.02}$	$0.03^{+0.17}_{-0.01}$
single top	$0.2^{+0.1}_{-0.2}$	0.4 ± 0.2
WW, WZ, ZZ	0.9 ± 0.2	0.7 ± 0.3
$Z\gamma$	0.2 ± 0.1	0.3 ± 0.1
$Z+\text{jets}$	0.8 ± 0.7	0.1 ± 0.1
diphoton	$0.5^{+0.7}_{-0.5}$	–
$\gamma+\text{jets}$	0.1 ± 0.3	–
total predicted	13.0 ± 3.4	15.1 ± 3.6
data	15	11

Table 4: Numbers of expected background and observed data events in the SR. The uncertainties include statistical and systematic effects.

Systematic	Electron Channel		Muon Channel	
	1500, 200	600, 500	1500, 200	600, 500
trigger	2.0 %		2.0 %	
lepton identification	1.9 %		0.4 %	
photon identification	4.6 %		4.6 %	
photon p_{T} requirement	1.2 %	0.2 %	1.4 %	0.1 %
$E_{\mathrm{T}}^{\mathrm{miss}}$, m_{T}	+6.1 % -7.5 %	2.2 %	+5.4 % -5.5 %	+0.0 % -0.8 %
Total	+8.2 % -9.3 %	5.8 %	+7.4 % -7.5 %	+7.5 % -7.6 %
Theory	3.9 %	19.4 %	3.9 %	19.4 %

Table 5: A summary of the systematic uncertainties on the signal efficiency times acceptance for two characteristic points in the parameter space. The $m(\tilde{g}) = 1500\,\mathrm{GeV}$, $m(\tilde{\chi}_1^0) = 200\,\mathrm{GeV}$ point is a representative point for electroweak production while the $m(\tilde{g}) = 600\,\mathrm{GeV}$, $m(\tilde{\chi}_1^0) = 500\,\mathrm{GeV}$ point is representative for strong production. Also included is the theoretical uncertainty of the two points.

7 Results

Table 4 shows the yields in the signal region including systematic uncertainties, and Fig. 5 shows the $E_{\mathrm{T}}^{\mathrm{miss}}$ and m_{T} distributions in the signal regions. No excess is seen.

Limits were extracted using the CL_s prescription [75] with a profile log-likelihood ratio test. Uncertainties on the background and signal expectations were treated as Gaussian-distributed nuisance parameters in the maximum likelihood fit. The electron and muon channels were treated as independent channels and were combined statistically for the model-dependent limit setting. Uncertainties of the same type, for example, on the photon reconstruction, were considered to be correlated between the two channels. Furthermore, uncertainties of the same type were considered to be correlated for all the different MC samples, whether background or signal.

Treating the electron and muon channels separately, it was found that visible cross sections, defined as the production cross section times efficiency times acceptance, above 2.7 fb (1.8 fb) in the electron (muon) channel can be excluded at 95 % CL. These two channels were also combined to set limits in the GGM scenario with a wino-like NLSP. Figure 6 shows the results in the plane of gluino mass versus wino mass. Three contours are shown for the observed limits, corresponding to the nominal SUSY production cross section as well as those derived by reducing and increasing the cross section by one standard deviation of the combined theoretical uncertainty (the combined uncertainty due to the PDFs and renormalisation and factorisation scales). It was found that gluinos masses below 619 GeV were excluded at 95 % CL for any wino mass less than the excluded gluino mass. Wino masses less than 221 GeV were excluded at 95 % CL for any value of the gluino mass.

8 Conclusions

A search for SUSY in events with at least one photon, at least one electron or muon, and substantial $E_{\mathrm{T}}^{\mathrm{miss}}$ is presented. The search for the electron (muon) signature was performed using 4.8 fb^{-1} (4.7 fb^{-1}) of 7 TeV pp collision data recorded with the ATLAS detector at the LHC. No excess of events was observed above the Standard Model prediction and model-independent exclusion limits for new physics were set. In addition, in the context of a generalized model of gauge-mediated supersymmetry breaking featuring production of gluino pairs and a wino-like next-to-lightest supersymmetric partner, gluinos masses below 619 GeV were excluded for any wino mass less than the excluded gluino mass. For the same model, the lack of observation of direct gaugino production excludes wino masses of less than 221 GeV for any value of the gluino mass.

9 Acknowledgements

We thank CERN for the very successful operation of the LHC, as well as the support staff from our institutions without whom ATLAS could not be operated efficiently.

We acknowledge the support of ANPCyT, Argentina; YerPhI, Armenia; ARC, Australia; BMWF and FWF, Austria; ANAS, Azerbaijan; SSTC, Belarus; CNPq and FAPESP, Brazil; NSERC, NRC and CFI, Canada; CERN; CONICYT, Chile; CAS, MOST and NSFC, China; COLCIENCIAS, Colombia; MSMT CR, MPO CR and VSC CR, Czech Republic; DNRF, DNSRC and Lundbeck Foundation, Denmark; EPLANET and ERC, European Union; IN2P3-CNRS, CEA-DSM/IRFU, France; GNSF, Georgia; BMBF, DFG, HGF, MPG and AvH Foundation, Germany; GSRT, Greece; ISF, MINERVA, GIF, DIP and Benoziyo Center, Israel; INFN, Italy; MEXT and JSPS, Japan; CNRST, Morocco; FOM and NWO, Netherlands; RCN, Norway; MNiSW, Poland; GRICES and FCT, Portugal; MERYS (MECTS), Romania; MES of Russia and ROSATOM, Russian Federation; JINR; MSTD, Serbia; MSSR, Slovakia; ARRS

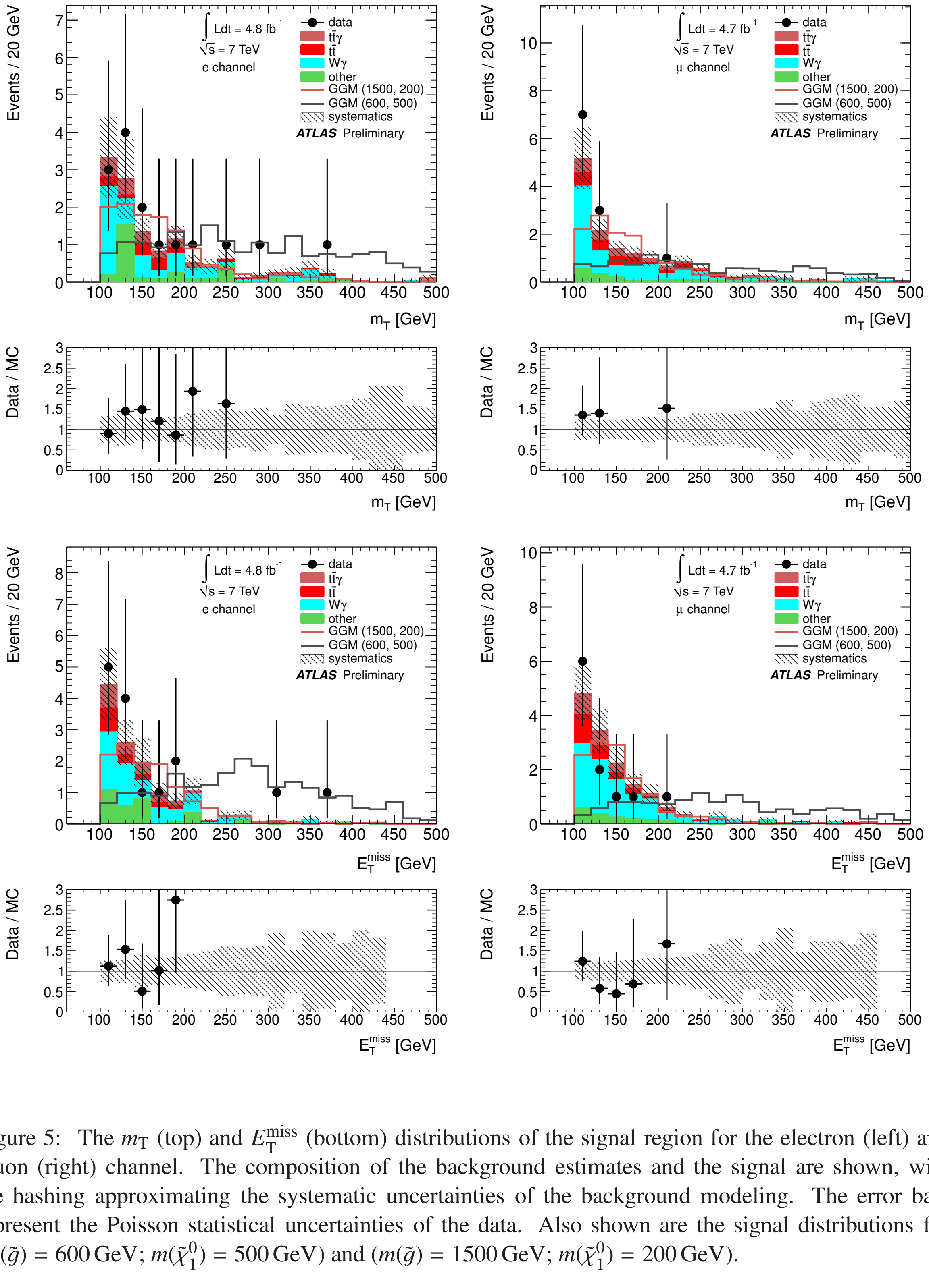

Figure 5: The m_{T} (top) and $E_{\mathrm{T}}^{\mathrm{miss}}$ (bottom) distributions of the signal region for the electron (left) and muon (right) channel. The composition of the background estimates and the signal are shown, with the hashing approximating the systematic uncertainties of the background modeling. The error bars represent the Poisson statistical uncertainties of the data. Also shown are the signal distributions for ($m(\tilde{g})$ = 600 GeV; $m(\tilde{\chi}_1^0)$ = 500 GeV) and ($m(\tilde{g})$ = 1500 GeV; $m(\tilde{\chi}_1^0)$ = 200 GeV).

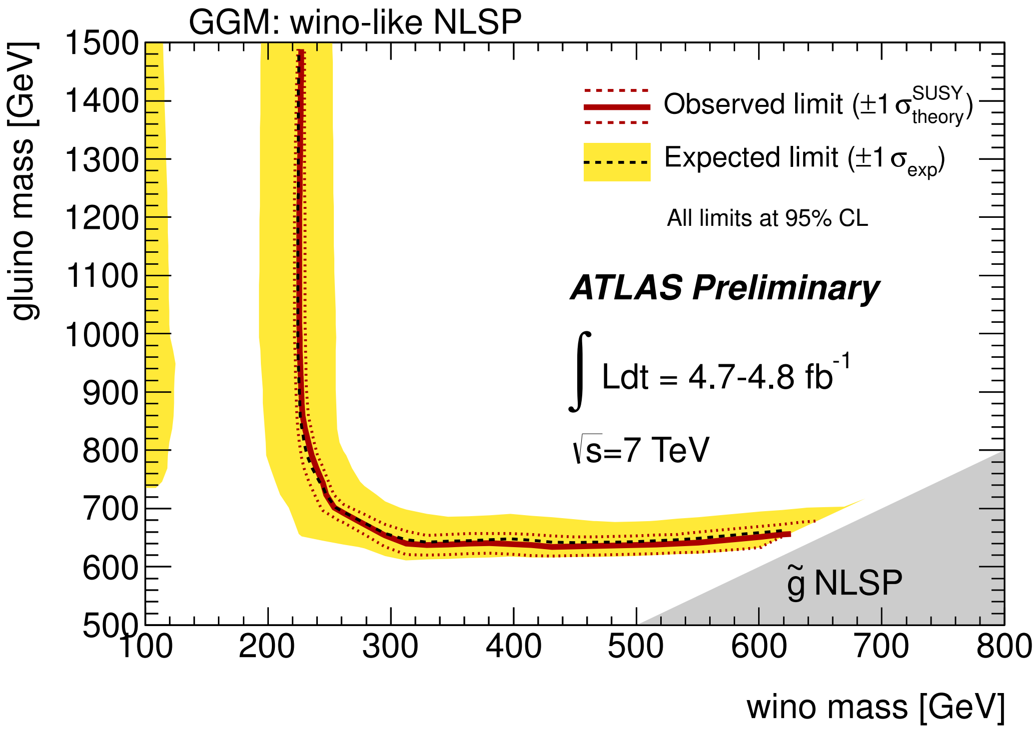

Figure 6: The expected and observed limits on the GGM grid with a wino-like NLSP.

and MVZT, Slovenia; DST/NRF, South Africa; MICINN, Spain; SRC and Wallenberg Foundation, Sweden; SER, SNSF and Cantons of Bern and Geneva, Switzerland; NSC, Taiwan; TAEK, Turkey; STFC, the Royal Society and Leverhulme Trust, United Kingdom; DOE and NSF, United States of America.

The crucial computing support from all WLCG partners is acknowledged gratefully, in particular from CERN and the ATLAS Tier-1 facilities at TRIUMF (Canada), NDGF (Denmark, Norway, Sweden), CC-IN2P3 (France), KIT/GridKA (Germany), INFN-CNAF (Italy), NL-T1 (Netherlands), PIC (Spain), ASGC (Taiwan), RAL (UK) and BNL (USA) and in the Tier-2 facilities worldwide.

References

[1] H. Miyazawa, *Baryon Number Changing Currents*, Prog. Theor. Phys. **36 (6)** (1966) 1266–1276.

[2] P. Ramond, *Dual Theory for Free Fermions*, Phys. Rev. **D3** (1971) 2415–2418.

[3] Y. A. Golfand and E. P. Likhtman, *Extension of the Algebra of Poincare Group Generators and Violation of p Invariance*, JETP Lett. **13** (1971) 323–326.

[4] A. Neveu and J. H. Schwarz, *Factorizable dual model of pions*, Nucl. Phys. **B31** (1971) 86–112.

[5] A. Neveu and J. H. Schwarz, *Quark Model of Dual Pions*, Phys. Rev. **D4** (1971) 1109–1111.

[6] J.-L. Gervais and B. Sakita, *Field theory interpretation of supergauges in dual models*, Nucl. Phys. **B34** (1971) 632–639.

[7] D. V. Volkov and V. P. Akulov, *Is the Neutrino a Goldstone Particle?*, Phys. Lett. **B46** (1973) 109–110.

[8] J. Wess and B. Zumino, *A Lagrangian Model Invariant Under Supergauge Transformations*, Phys. Lett. **B49** (1974) 52.

[9] J. Wess and B. Zumino, *Supergauge Transformations in Four-Dimensions*, Nucl. Phys. **B70** (1974) 39–50.

[10] P. Fayet, *Supersymmetry and Weak, Electromagnetic and Strong Interactions*, Phys. Lett. **B64** (1976) 159.

[11] P. Fayet, *Spontaneously Broken Supersymmetric Theories of Weak, Electromagnetic and Strong Interactions*, Phys. Lett. **B69** (1977) 489.

[12] G. R. Farrar and P. Fayet, *Phenomenology of the Production, Decay, and Detection of New Hadronic States Associated with Supersymmetry*, Phys. Lett. **B76** (1978) 575–579.

[13] P. Fayet, *Relations Between the Masses of the Superpartners of Leptons and Quarks, the Goldstino Couplings and the Neutral Currents*, Phys. Lett. **B84** (1979) 416.

[14] S. Dimopoulos and H. Georgi, *Softly Broken Supersymmetry and SU(5)*, Nucl. Phys. **B193** (1981) 150.

[15] M. Dine and W. Fischler, *A Phenomenological Model of Particle Physics Based on Supersymmetry*, Phys. Lett. **B110** (1982) 227.

[16] L. Alvarez-Gaume, M. Claudson, and M. Wise, *Low-Energy Supersymmetry*, Nucl. Phys. **B207** (1982) 96.

[17] C. R. Nappi and B. A. Ovrut, *Supersymmetric Extension of the SU(3) x SU(2) x U(1) Model*, Phys. Lett. **B113** (1982) 175.

[18] M. Dine and A. Nelson, *Dynamical supersymmetry breaking at low-energies*, Phys. Rev. **D48** (1993) 1277, `hep-ph/9303230`.

[19] M. Dine, A. Nelson, and Y. Shirman, *Low-energy dynamical supersymmetry breaking simplified*, Phys. Rev. **D51** (1995) 1362, `hep-ph/9408384`.

[20] M. Dine, A. Nelson, Y.Nir, and Y. Shirman, *New tools for low-energy dynamical supersymmetry breaking*, Phys. Rev. **D53** (1996) 2658, `hep-ph/9507378`.

[21] P. Meade, N. Seiberg, and D. Shih, *General Gauge Mediation*, Prog. Theor. Phys. Suppl. **177** (2009) 143–158, `arXiv:0801.3278 [hep-ph]`.

[22] M. Buican, P. Meade, N. Seiberg, and D. Shih, *Exploring General Gauge Mediation*, JHEP **03** (2009) 016, `arXiv:0812.3668 [hep-ph]`.

[23] J. T. Ruderman and D. Shih, *General Neutralino NLSPs at the Early LHC*, `arXiv:1103.6083 [hep-ph]`.

[24] CMS Collaboration, *Search for supersymmetry in events with a lepton, a photon, and large missing transverse energy in pp collisions at* $\sqrt{s} = 7$ TeV, JHEP **06** (2011) 093, `arXiv:1105.3152 [hep-ex]`.

[25] ATLAS Collaboration, *The ATLAS Experiment at the CERN Large Hadron Collider*, JINST **3** (2008) S08003.

[26] ATLAS Collaboration, *Performance of the ATLAS Trigger System in 2010*, Eur.Phys.J. **C72** (2012) 1849, `arXiv:1110.1530 [hep-ex]`.

[27] A. Djouadi, J.-L. Kneur, and G. Moultaka, *SuSpect: A Fortran code for the supersymmetric and Higgs particle spectrum in the MSSM*, Comput.Phys.Commun. **176** (2007) 426–455, `arXiv:hep-ph/0211331 [hep-ph]`.

[28] M. Muhlleitner, A. Djouadi, and Y. Mambrini, *SDECAY: A Fortran code for the decays of the supersymmetric particles in the MSSM*, Comput.Phys.Commun. **168** (2005) 46–70, `arXiv:hep-ph/0311167 [hep-ph]`.

[29] A. Djouadi, J. Kalinowski, and M. Spira, *HDECAY: A Program for Higgs boson decays in the standard model and its supersymmetric extension*, Comput.Phys.Commun. **108** (1998) 56–74, `arXiv:hep-ph/9704448 [hep-ph]`.

[30] M. Bahr et al., *Herwig++ Physics and Manual*, Eur. Phys. J. **C58** (2008) 639–707, `arXiv:0803.0883 [hep-ph]`.

[31] W. Beenakker, R. Hopker, M. Spira, and P. Zerwas, *Squark and gluino production at hadron colliders*, Nucl.Phys. **B492** (1997) 51–103, `arXiv:hep-ph/9610490 [hep-ph]`.

[32] A. Kulesza and L. Motyka, *Threshold resummation for squark-antisquark and gluino-pair production at the LHC*, Phys.Rev.Lett. **102** (2009) 111802, `arXiv:0807.2405 [hep-ph]`.

[33] A. Kulesza and L. Motyka, *Soft gluon resummation for the production of gluino-gluino and squark-antisquark pairs at the LHC*, Phys.Rev. **D80** (2009) 095004, `arXiv:0905.4749 [hep-ph]`.

[34] W. Beenakker, S. Brensing, M. Kramer, A. Kulesza, E. Laenen, et al., *Soft-gluon resummation for squark and gluino hadroproduction*, JHEP **0912** (2009) 041, `arXiv:0909.4418 [hep-ph]`.

[35] W. Beenakker, S. Brensing, M. Kramer, A. Kulesza, E. Laenen, et al., *Squark and Gluino Hadroproduction*, Int.J.Mod.Phys. **A26** (2011) 2637–2664, `arXiv:1105.1110 [hep-ph]`.

[36] M. Kramer, A. Kulesza, R. van der Leeuw, M. Mangano, S. Padhi, et al., *Supersymmetry production cross sections in pp collisions at* $\sqrt{s} = 7$ *TeV*, `arXiv:1206.2892 [hep-ph]`.

[37] M. L. Mangano, M. Moretti, F. Piccinini, R. Pittau, and A. D. Polosa, *ALPGEN, a generator for hard multiparton processes in hadronic collisions*, JHEP **0307** (2003) 001, `arXiv:hep-ph/0206293 [hep-ph]`.

[38] D. Stump et al., *Inclusive jet production, parton distributions, and the search for new physics*, JHEP **10** (2003) 046, `arXiv:hep-ph/0303013`.

[39] ATLAS Collaboration, *Measurement of* $W\gamma$ *and* $Z\gamma$ *production cross sections in pp collisions at* $\sqrt{s} = 7\,\text{TeV}$ *and limits on anomalous triple gauge couplings with the ATLAS detector*, `arXiv:1205.2531 [hep-ex]`.

[40] W. Kilian, T. Ohl, and J. Reuter, *WHIZARD: Simulating Multi-Particle Processes at LHC and ILC*, Eur.Phys.J. **C71** (2011) 1742, `arXiv:0708.4233 [hep-ph]`.

[41] P. Golonka and Z. Was, *PHOTOS Monte Carlo: A Precision tool for QED corrections in Z and W decays*, Eur.Phys.J. **C45** (2006) 97–107, `arXiv:hep-ph/0506026 [hep-ph]`.

[42] ATLAS Collaboration, *Measurement of the inclusive $t\bar{t}\gamma$ cross section with the ATLAS detector*, ATLAS-CONF-2011-153, Nov, 2011. `https://cdsweb.cern.ch/record/1398197`.

[43] S. Frixione and B. R. Webber, *The MC@NLO 3.2 event generator*, `arXiv:hep-ph/0601192`.

[44] S. Frixione and B. R. Webber, *Matching NLO QCD computations and parton shower simulations*, JHEP **06** (2002) 029, `arXiv:hep-ph/0204244`.

[45] P. M. Nadolsky, H.-L. Lai, Q.-H. Cao, J. Huston, J. Pumplin, et al., *Implications of CTEQ global analysis for collider observables*, Phys.Rev. **D78** (2008) 013004, `arXiv:0802.0007 [hep-ph]`.

[46] M. Aliev, H. Lacker, U. Langenfeld, S. Moch, P. Uwer, et al., *HATHOR: HAdronic Top and Heavy quarks crOss section calculatoR*, Comput.Phys.Commun. **182** (2011) 1034–1046, `arXiv:1007.1327 [hep-ph]`.

[47] A. Martin, W. Stirling, R. Thorne, and G. Watt, *Parton distributions for the LHC*, Eur.Phys.J. **C63** (2009) 189–285, `arXiv:0901.0002 [hep-ph]`.

[48] T. Gleisberg, S. Hoeche, F. Krauss, M. Schonherr, S. Schumann, et al., *Event generation with SHERPA 1.1*, JHEP **0902** (2009) 007, `arXiv:0811.4622 [hep-ph]`.

[49] H.-L. Lai, M. Guzzi, J. Huston, Z. Li, P. M. Nadolsky, et al., *New parton distributions for collider physics*, Phys.Rev. **D82** (2010) 074024, `arXiv:1007.2241 [hep-ph]`.

[50] C. Anastasiou, L. J. Dixon, K. Melnikov, and F. Petriello, *High precision QCD at hadron colliders: Electroweak gauge boson rapidity distributions at NNLO*, Phys. Rev. **D69** (2004) 094008, `arXiv:hep-ph/0312266`.

[51] B. P. Kersevan and E. Richter-Was, *The Monte Carlo event generator AcerMC version 2.0 with interfaces to PYTHIA 6.2 and HERWIG 6.5*, `arXiv:hep-ph/0405247 [hep-ph]`.

[52] A. Sherstnev and R. Thorne, *Different PDF approximations useful for LO Monte Carlo generators*, `arXiv:0807.2132 [hep-ph]`.

[53] N. Kidonakis, *Two-loop soft anomalous dimensions for single top quark associated production with a W^- or H^-*, Phys.Rev. **D82** (2010) 054018, `arXiv:1005.4451 [hep-ph]`.

[54] N. Kidonakis, *Next-to-next-to-leading-order collinear and soft gluon corrections for t-channel single top quark production*, Phys.Rev. **D83** (2011) 091503, `arXiv:1103.2792 [hep-ph]`.

[55] J. M. Campbell, R. K. Ellis, and C. Williams, *Vector boson pair production at the LHC*, JHEP **1107** (2011) 018, `arXiv:1105.0020 [hep-ph]`.

[56] T. Sjostrand, S. Mrenna, and P. Skands, *PYTHIA 6.4 physics and manual*, JHEP **05** (2006) 026, `arXiv:hep-ph/0603175`.

[57] G. Corcella et al., *HERWIG 6: An event generator for hadron emission reactions with interfering gluons (including supersymmetric processes)*, JHEP **01** (2001) 010, `arXiv:hep-ph/0011363`.

[58] G. Corcella et al., *HERWIG 6.5 release note*, `arXiv:hep-ph/0210213 [hep-ph]`.

[59] ATLAS Collaboration, *ATLAS tunes of PYTHIA 6 and Pythia 8 for MC11*, ATL-PHYS-PUB-2011-009, CERN, Geneva, Jul, 2011.

[60] J. F. J. Butterworth and M. Seymour, *Multiparton interactions in photoproduction at HERA*, Z. Phys. **C72** (1996) 637–646, `hep-ph/9601371`.

[61] GEANT4 Collaboration, S. Agostinelli et al., *GEANT4: A simulation toolkit*, Nucl. Instrum. Meth. **A506** (2003) 250–303.

[62] ATLAS Collaboration, *The ATLAS Simulation Infrastructure*, Eur. Phys. J. **C70** (2010) 823–874, `arXiv:1005.4568 [physics.ins-det]`.

[63] ATLAS Collaboration, *Measurements of the photon identification efficiency with the ATLAS detector using* $4.9\,fb^{-1}$ *of pp collision data collected in 2011*, ATLAS-CONF-2012-123, Aug, 2012. `https://cdsweb.cern.ch/record/1473426`.

[64] ATLAS Collaboration, *Electron performance measurements with the ATLAS detector using the 2010 LHC proton-proton collision data*, Eur.Phys.J. **C72** (2012) 1909, `arXiv:1110.3174 [hep-ex]`.

[65] ATLAS Collaboration, *Muon reconstruction efficiency in reprocessed 2010 LHC proton-proton collision data recorded with the ATLAS detector*, ATLAS-CONF-2011-063, Apr, 2011. `https://cdsweb.cern.ch/record/1345743`.

[66] M. Cacciari, G. Salam, and G. Soyez, *The anti-*k_t *jet clustering algorithm*, JHEP **04** (2008) 063, `arXiv:0802.1189 [hep-ph]`.

[67] ATLAS Collaboration Collaboration, *Jet energy measurement with the ATLAS detector in proton-proton collisions at* $\sqrt{s} = 7\,\text{TeV}$, `arXiv:1112.6426 [hep-ex]`.

[68] ATLAS Collaboration, *Performance of Missing Transverse Momentum Reconstruction in Proton-Proton Collisions at 7 TeV with ATLAS*, Eur.Phys.J. **C72** (2012) 1844, `arXiv:1108.5602 [hep-ex]`.

[69] ATLAS Collaboration, *Further search for supersymmetry at* $\sqrt{s} = 7\,\text{TeV}$ *in final states with jets, missing transverse momentum and isolated leptons with the ATLAS detector*, `arXiv:1208.4688 [hep-ex]`.

[70] ATLAS Collaboration, *Luminosity Determination in pp Collisions at* $\sqrt{s} = 7\,\text{TeV}$ *using the ATLAS Detector in 2011*, ATLAS-CONF-2011-116, Jul, 2011. `http://cdsweb.cern.ch/record/1367408`.

[71] ATLAS Collaboration, *Luminosity Determination in pp Collisions at* $\sqrt{s} = 7$ *TeV Using the ATLAS Detector at the LHC*, Eur.Phys.J. **C71** (2011) 1630, `arXiv:1101.2185 [hep-ex]`.

[72] K. Melnikov, M. Schulze, and A. Scharf, *QCD corrections to top quark pair production in association with a photon at hadron colliders*, Phys.Rev. **D83** (2011) 074013, `arXiv:1102.1967 [hep-ph]`.

[73] ATLAS Collaboration, *Search for diphoton events with large missing transverse momentum in 7 TeV proton-proton collision data with the ATLAS detector*, `arXiv:1209.0753 [hep-ex]`.

[74] ATLAS Collaboration. `https://twiki.cern.ch/twiki/pub/AtlasPublic/MuonPerformancePublicPlots/ATL-COM-PHYS-2011-1504.pdf`.

[75] A. L. Read, *Presentation of search results: The* CL_s *technique*, J.Phys.G **G28** (2002) 2693.